Comparing critical source areas for the sediment and nutrients of calibrated and uncalibrated models in a plateau watershed in southwest China

Journal of Environmental Management

Chen, Meijun; Janssen, Annette B.G.; de Klein, Jeroen J.M.; Du, Xinzhong; Lei, Qiuliang et al

https://doi.org/10.1016/j.jenvman.2022.116712

Journal of Environmental Management 326 (2023) 116712

Contents lists available at ScienceDirect

Journal of Environmental Management

journal homepage: www.elsevier.com/locate/jenvman

Review

Comparing critical source areas for the sediment and nutrients of calibrated and uncalibrated models in a plateau watershed in southwest China

Meijun Chen [a,b,c], Annette B.G. Janssen [b], Jeroen J.M. de Klein [c], Xinzhong Du [a,*], Qiuliang Lei [a], Ying Li [d], Tianpeng Zhang [a], Wei Pei [a], Carolien Kroeze [b], Hongbin Liu [a,**]

[a] Institute of Agricultural Resources and Regional Planning, Chinese Academy of Agricultural Sciences/Key Laboratory of Nonpoint Source Pollution Control, Ministry of Agriculture and Rural Affairs, Beijing, 100081, China
[b] Water Systems and Global Change Group, Department of Environmental Sciences, Wageningen University and Research, PO Box 47, 6700AA Wageningen, the Netherlands
[c] Aquatic Ecology and Water Quality Management Group, Department of Environmental Sciences, Wageningen University and Research, PO Box, 47, 6700AA, Wageningen, the Netherlands
[d] State Key Laboratory of Resources and Environmental Information System, Institute of Geographic Sciences and Natural Resources Research, CAS, Beijing 100101, PR China

ARTICLE INFO

Keywords:
Soil and water assessment tool (SWAT)
Data scarcity
Model calibration
Seasonal
Yearly
Hydrology

ABSTRACT

Controlling non-point source pollution is often difficult and costly. Therefore, focusing on areas that contribute the most, so-called critical source areas (CSAs), can have economic and ecological benefits. CSAs are often determined using a modelling approach, yet it has proved difficult to calibrate the models in regions with limited data availability. Since identifying CSAs is based on the relative contributions of sub-basins to the total load, it has been suggested that uncalibrated models could be used to identify CSAs to overcome data scarcity issues. Here, we use the SWAT model to study the extent to which an uncalibrated model can be applied to determine CSAs. We classify and rank sub-basins to identify CSAs for sediment, total nitrogen (TN), and total phosphorus (TP) in the Fengyu River Watershed (China) with and without model calibration. The results show high similarity (81%–93%) between the identified sediment and TP CSA number and locations before and after calibration both on the yearly and seasonal scale. For TN alone, the results show moderate similarity on the yearly scale (73%). This may be because, in our study area, TN is determined more by groundwater flow after calibration than by surface water flow. We conclude that CSA identification with the uncalibrated model for TP is always good because its CSA number and locations changed least, and for sediment, it is generally satisfactory. The use of the uncalibrated model for TN is acceptable, as its CSA locations did not change after calibration; however, the TN CSA number changed by over 60% compared to the figures before calibration on both yearly and seasonal scales. Therefore, we advise using an uncalibrated model to identify CSAs for TN only if water yield composition changes are expected to be limited. This study shows that CSAs can be identified based on relative loading estimates with uncalibrated models in data-deficient regions.

1. Introduction

Excess amounts of nutrients are lost from watersheds, causing the deterioration of water quality in rivers, lakes, and seas (Janssen et al., 2017; Strokal et al., 2017; Tong et al., 2017a; Wang et al., 2020). Nutrient inputs to receiving water bodies can be divided into point sources and non-point sources. Point source pollution is relatively easy to manage because the source is discharged at one specific location, such as a sewage treatment plant. In contrast, non-point source (NPS) pollution is diffuse, making it difficult to observe and control (Chen et al., 2019; Li et al., 2019a; Tong et al., 2017b; Wang et al., 2019; Yang et al., 2019). Diffuse sources primarily include synthetic fertilizer, animal manure, and uncollected human waste. NPS pollution is a severe threat to the global water environment because it contributes to excessive N and P loading, which is mainly driven by hydrological processes such as groundwater flow, rainfall, and streamflow (Hanjra and Qureshi,

* Corresponding author.
** Corresponding author.
E-mail addresses: meijun.chen@wur.nl (M. Chen), duxinzhong@caas.cn (X. Du), liuhongbin@caas.cn (H. Liu).

https://doi.org/10.1016/j.jenvman.2022.116712
Received 22 June 2022; Received in revised form 24 October 2022; Accepted 3 November 2022
Available online 17 November 2022

2010; Peters and Meybeck, 2000). It is essential to study how to effectively decrease the risk of non-point nutrient loss in the hydrological cycle due to variations in climate and human factors that might affect water quality.

Implementing management measures to reduce nutrient loss in the entire watershed is often infeasible from an economic perspective (Sharpley et al., 2011). However, in most watersheds, a small land area often causes a disproportionately large amount of pollution (Pionke et al., 2000; White et al., 2009). These areas, called critical source areas (CSAs), result from an interaction between transport and pollution source factors, such as locations with concentrated agricultural activities adjacent to the receiving water bodies (Ouyang et al., 2008; Pionke et al., 2000; Strauss et al., 2007). Agricultural non-point source pollution management should target these areas that pollute the most to increase economic feasibility.

CSAs can be identified in different ways: (1) observation methods, (2) empirical methods, and (3) mechanistic model methods. First, observation methods directly measure pollution, which is challenging because the diffuse nature of NPS pollution, makes it difficult to observe (Pionke et al., 2000). Moreover, direct observations often require an ample workforce, material resources, and financial support. Second, empirical methods estimate the main nutrient source areas based on landscape and catchment characteristics (Andersen and Kronvang, 2006; Drewry et al., 2009; Ghebremichael et al., 2010; Sharpley et al., 2012), such as the phosphorus index (PI) method or the output coefficient method (Tong et al., 2021; Wu et al., 2015). The PI method is used to assess the risk of phosphorus losses, including soil erosion and nutrient transport (Ou and Wang, 2008; Ros et al., 2019). The output coefficient method, meanwhile, calculates the amount of pollutants by multiplying each separate source with an empirical coefficient. Both methods are unsuitable for identifying CSAs; the former focuses on risks rather than actual losses (White et al., 2009), and the latter is known for large errors (Rudra et al., 2020; Wu et al., 2015). Third, mechanistic models simulate nutrient losses, and many researchers have used them to identify CSAs in watersheds, such as the Areal Nonpoint Source Watershed Environment Response Simulation (ANSWERS; Bouraoui and Dillaha, 1996), the Agricultural Non-Point Source Pollution (AGNPS) model (Han et al., 2010), the Generalized Watershed Loading Function (GWLF; Niraula et al., 2013), and the Soil Water Assessment Tool (SWAT; Neitsch et al., 2011). The use of mechanistic models can avoid most limitations associated with observation and empirical methods and can help identify and prioritize sub-basins for the cost-effective implementation of management practices. An often-reported limitation of model methods is that they are highly dependent on observed data for calibration to obtain reliable simulations (Rudra et al., 2020). However, as identifying CSAs is based on the relative contributions of sub-basins to the total nutrient loads, it has been suggested that a model without calibration can also be used to identify CSAs. Niraula et al. (2012) have shown almost no change in CSA locations before and after calibration.

The ability to apply uncalibrated models can be of great importance for regions with data that is limited or difficult to measure (Davies, 2019; Janssen et al., 2019; Rozalis et al., 2010). While previous studies have already shown that uncalibrated watershed models can also identify CSAs on a yearly scale, the consistency in locations of CSAs under different hydrological conditions, with and without calibration, remains unknown. CSAs can change spatial-temporally. For instance, it has been shown that warmer or cooler years and seasonal variability affect hydrological conditions, thereby changing the locations of CSAs (Guo et al., 2020; Wei et al., 2016). Although previous research has shown that different climates and seasons affect CSA location, it remains unclear whether these changes are consistent between model outputs before and after calibration. When the model parameters are systematically adjusted over the entire watershed during calibration, the relative loadings of pollutants each sub-basin contribute may be affected (Rudra et al., 2020). Therefore, it is also necessary to study whether all sub-basins change similarly after calibration or whether some are more sensitive to parameter changes.

Here, we aim to study the consistency of CSAs at the sub-basin scale under different hydrological conditions and explore the impact of model calibration on the identification of CSAs. This study hypothesizes that uncalibrated models can be used to identify CSAs on a basin scale both seasonally and yearly under different hydrological conditions because CSA identification is based on relative contributions. To confirm this hypothesis, we apply both calibrated and uncalibrated SWAT models to the Fengyu River Watershed as a case study. We then evaluate the changes in CSA locations and identify the important factors that affect the difference between calibrated and uncalibrated models. This study can provide helpful guidelines for CSA identification in data-limited regions through a better understanding of the effect of model calibration on identifying CSAs.

2. Materials and methods

In our analysis, we 1) establish a SWAT model based on the available data and obtain the simulation results with and without model calibration; 2) compare the sub-basins' contribution change, CSA location change, and the CSAs' change in percentage before and after calibration; and 3) assess the uncalibrated model's feasibility in identifying CSAs and investigate possible reasons for the infeasibilities.

2.1. Study area description

We use the Fengyu River Watershed as our case study. Its drainage area is 219 km^2, and it forms one of the main water and nutrient sources of Erhai Lake, the second-largest plateau freshwater lake of Yunnan Province in Southwestern China (Fig. 1; Li et al., 2019b). Erhai Lake is the primary source of drinking water for the local people. Since the 1980s, the human population has rapidly increased, and fast economic development has led to several ecological problems in Erhai Lake (Li et al., 2019a). The nutrient losses from agricultural production and domestic wastewater are directly discharged into the lake, resulting in water quality deterioration (Ji et al., 2017; Li et al., 2020; Peng et al., 2018). The water quality of the lake became eutrophic in recent years, and it fluctuated between level II (suitable for fishing and bathing) and level III (a moderate level of eutrophication) water quality according to the Chinese standard (GB3838-2002, 2002). Large-scale cyanobacteria blooms occurred in Erhai Lake in 1996, 2003, and 2013 (Lin et al., 2020). The Fengyu River Watershed is a typical agricultural sub-basin of the Erhai Basin. The watershed has an elevation of 2072 m–3623 m above sea level and contains many mountainous streams and springs. It has a subtropical monsoon climate with distinct dry and wet seasons. The annual average temperature is 13.9 °C, and the average yearly rainfall is 745 mm. The flood season is from June to October and accounts for about 85% of the annual rainfall (Li et al., 2019b). The agricultural calendar distinguishes between two seasons: an early season from October to April and a late one from May to September. During the early season, both the precipitation and temperature are relatively low, which is suitable for planting rape, broad beans, and wheat. During the late season, the rainfall is abundant, and temperatures rise, so staple food such as rice, corn, and a variety of vegetables can achieve a high yield. In the upstream part of the watershed, flue-cured tobacco is primarily grown in the late season.

2.2. SWAT model setup

Based on the digital elevation map (DEM), the Fengyu River Watershed is subdivided into 37 sub-basins, and each is further divided into HRUs. The key processes of SWAT occur on the scale of HRUs (Niraula et al., 2013). The SWAT input data is divided into geographical data, climatological data, and management data. The geographical data used to construct the SWAT model includes the DEM, the soil type map, the land use map, and the drainage system map. For each HRU, the

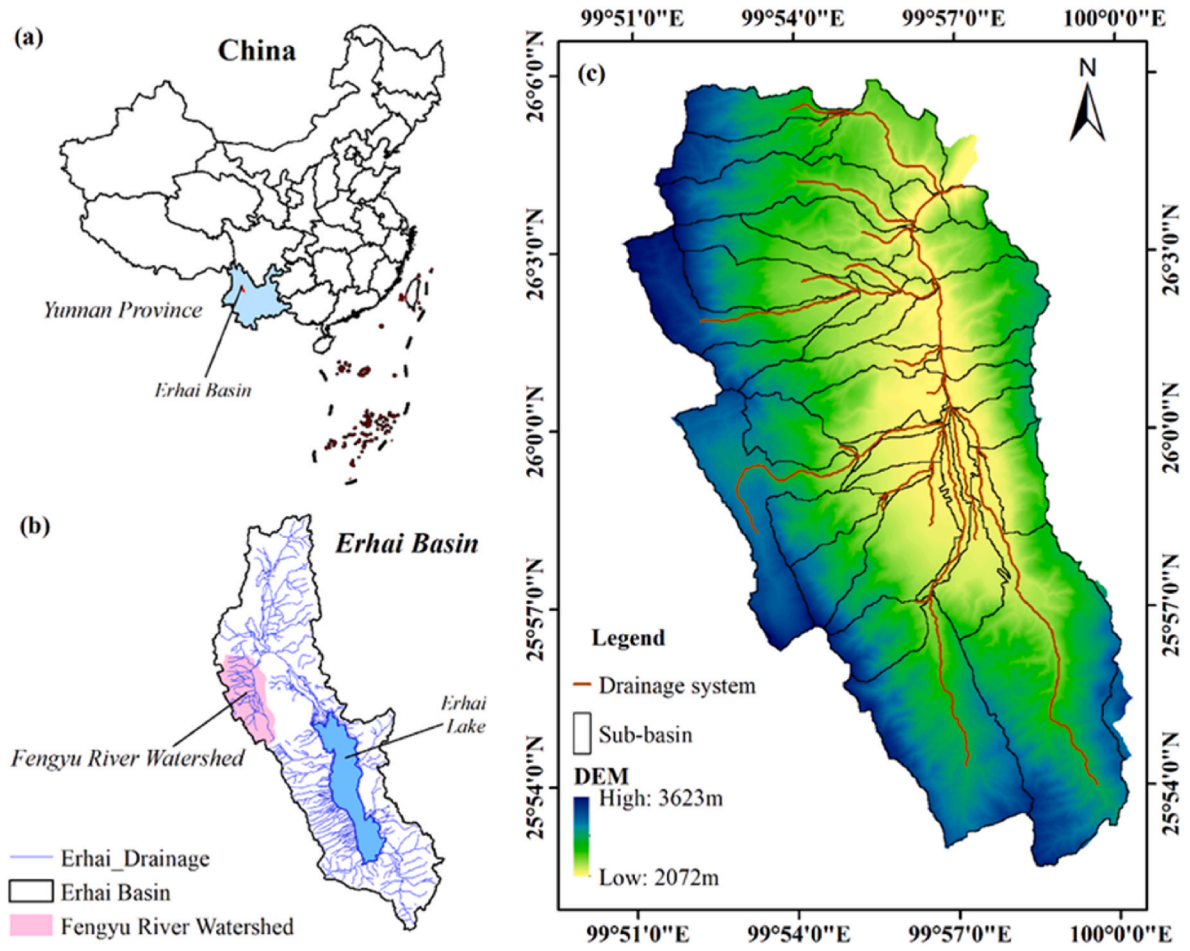

Fig. 1. The study area: (a) the location of Yunnan Province in China; (b) the location of the Fengyu River Watershed and Erhai Lake. The Fengyu River Watershed is one of the main water and nutrient sources within the Erhai Basin; (c) the Fengyu River Watershed, which is divided into 37 sub-basins.

geometric features are defined. Climate data include precipitation, temperature, relative humidity, radiation hours, and wind speed data at the outlet monitoring station. Management data includes farmland management data and agricultural activities (Table S1). Each season's agricultural activities are set for tillage, planting, fertilization, irrigation, harvest, and kill (Table S2).

2.3. SWAT model

SWAT is a semi-distributed model on a watershed scale. It is widely used to simulate water yield, sediment, nitrogen, phosphorus, and other substances over long periods and scenarios for different management practices (Neitsch et al., 2011). Nitrogen has two forms: organic and inorganic. Inorganic nitrogen is further separated into nitrate in the surface runoff, nitrate in the lateral flow, and nitrate in groundwater. Phosphorus calculation differs from that of nitrogen. It has three forms: organic phosphorus attached to sediment, inorganic phosphorus attached to sediment, and inorganic dissolved phosphorus in surface runoff. The basic unit used in the model is the hydrological response unit (HRU). Each sub-basin's water yield and pollutant load is transported to the watershed outlet or between sub-watersheds through the drainage network. The runoff and nutrient load of each sub-basin is the combined sum of all HRUs. For a more detailed description of the SWAT model processes, we refer to Neitsch et al. (2011).

2.4. Model calibration and validation

According to the actual situation of the watershed, we selected 42 parameters for calibration of flow, sediment, total nitrogen, and total phosphorus. Parameter sensitivity ranking, calibration, and validation results are presented in Table S3. We used the observed monthly streamflow, sediment, and water quality data of the watershed outlet monitoring station from January 2011 to February 2014 to calibrate and validate the model. As the whole study period covers three different years and two months, we decided to divide the study period into 2 parts; the first half is used for calibration and the second for validation (Table S4).

We applied the SUIF-2 optimization algorithm in SWAT-CUP 2012 (Abbaspour, 2013) software to calibrate the 42 parameters following the standard procedure according to Arnold et al. (2013). More than 10 iterations, each of which included 500–1500 simulations, were needed to obtain the final parameter range. In every iteration, we adjusted certain parameters to fit the actual situation. The Nash–Sutcliffe efficiency (NS), the coefficient of determination (R^2), and the percentage bias (Pbias; Moriasi et al., 2015) were used as statistics to evaluate the model performance. The NS ranges from negative infinity to 1 and assesses how well the model-to-data plot fits the 1:1 line. R^2 is used to measure the consistency of the trend between the measured data and the simulated value, and the Pbias is the ratio of absolute error (the difference between the measured data and the simulated data) to the measured value. The equations for the three measures are as follows:

$$R^2 = \left[\frac{\sum_{i=1}^{n}(O_i - \overline{O})(P_i - \overline{P})}{\sqrt{\sum_{i=1}^{n}(O_i - \overline{O})^2}\sqrt{\sum_{i=1}^{n}(P_i - \overline{P})^2}} \right]^2 \quad (1)$$

$$NSE = 1 - \frac{\sum_{i=1}^{n}(O_i - P_i)^2}{\sum_{i=1}^{n}(O_i - \overline{O})^2} \quad (2)$$

$$Pbias = \frac{\sum_{i=1}^{n} O_i - P_i}{\sum_{i=1}^{n} O_i} \times 100 \quad (3)$$

where P_i is the predicted (simulated) value for the constituent being evaluated, O_i is the observed (measured) value, $\overline{P}$ is the mean of the predicted value, $\overline{O}$ is the mean of the observed value, and n is the total number of observations. G_{NS} is the objective function:

$$G_{NS} = \sum w_j NS_j \quad (4)$$

where w_j is the weight of each variable j. We set the overall performance of streamflow, sediment, TN and TP as the objective function and weighted each with, respectively, 1, 1.5, 1, and 1. Since sediment is more difficult to calibrate, we put it at a higher weight to obtain a higher G_{NS} value. We used the criteria set by Moriasi et al. (2015) to evaluate the model performance qualitatively. We chose simultaneous calibration to optimize the four variables at the same time and obtained the best representation of the watershed model. We also used the SUIF-2 optimization algorithm from SWAT-CUP to conduct uncertainty analysis for the model simulations. The P-factor and R-factor for the 95% prediction uncertainty band obtained from SUFI-2 were used to evaluate model uncertainties for streamflow, sediment, and nutrient load simulations. The P-factor is the percentage of the observed data bracketed by the 95% uncertainty band, and the R-factor is the normalized width of the band (Chen et al., 2017; Du et al., 2019). If the P-factor is closer to 1, and the R-factor is closer to 0, it indicates that there is less uncertainty for the model simulation. We ran the calibration and validation periods for each variable with initial parameter ranges for each with 1000 simulations. After fixing the optimal parameters of runoff, we ran the sediment and then fixed the parameters of the sediment to run TN and TP.

2.5. Zonation method for CSAs

For the zonation of CSAs, our study divided sub-basins into five classes using the cumulative curve method (Guo et al., 2020; see Fig. S1). The cumulative curve method was used to classify the cumulative relative sediment and nutrient load of sub-basins into fixed intervals at both yearly and seasonal scales. We identified CSAs in two steps. In the first step, we used the sediment and nutrient load intensity of 37 sub-basins. Nutrient load intensity is defined as the sub-basin's sediment and nutrient output in mass per time unit divided by the surface area of sub-basins. The sub-basins' load intensity was sorted from large to small. In the second step, we calculated the cumulative load based on the sediment and nutrient load from each sub-basin. Nutrient load is defined as the sub-basin's sediment and nutrient output in mass per time unit. We utilized 20%, 40%, 60%, and 80% as the relative dividing points to divide the sub-basins into five risk level zones. The first two classes (the top 0%–40%) were defined as high-risk areas; the third class areas were defined as potential risk areas (the top 40%–60%); and the last two classes (60%–100%) were defined as low-risk areas. CSAs are those areas that fall within the high-risk and potential risk categories.

Since CSAs change spatially-temporally (Guo et al., 2020; Uribe et al., 2020; Wei et al., 2016), we aimed to identify how different hydrological conditions can affect CSAs at seasonal scales, as well. The analysis of the hydrological conditions could lead to an understanding of the inter-relationships among meteorological, surface- and ground-water, and physical and biological factors that influence the flow, quality, and/or timing of water (McLaughlin, 1997). Furthermore, the concept of hydrological conditions can also be an expression of changes in the magnitude, direction, and rate of different hydrological phenomena. Analyzing the changes of CSAs under different hydrological conditions is helpful for managers to control the NPS pollution in a watershed.

First, we analyzed the CSAs at a yearly scale and differentiated between wet, normal, and dry years. Hence, the frequency analysis method (Liu et al., 2020) was used. With this method, the hydrological P-III Frequency curve was created based on rainfall data from 2011 to 2017 (Table S5). Using the P-III curve (McMahon and Srikanthan, 1981), wet years, normal years, and dry years were defined respectively as the 0%–25% frequency, 25%–50% frequency, and 50%–75% frequency, respectively. Following this method, 2011 was a dry year, 2012 was a normal year, and 2013 was a wet year. Next, we analyzed CSAs on a seasonal scale and differentiated between flood seasons (June–October) and non-flood seasons (November–May). Accordingly, we had six hydrological conditions for the seasonal scale: dry year, flood season; dry year, non-flood season; normal year, flood season; normal year, non-flood season; wet year, flood season; and wet year, non-flood season. Each hydrological condition had 37 nutrient load simulations for all sub-basins, as we divided the Fengyu River Watershed into 37 sub-basins. To ensure the consistency of evaluation criteria, we evaluated the sub-basins together. Ultimately, we had 37 sub-basins with six hydrological seasons equaling 222 values.

2.6. Comparison and statistical analysis method

We compared the uncalibrated model results with the calibrated model results in three steps. First, the relative load contributions of the sub-basins calculated by the uncalibrated model were plotted against the contributions in the calibrated model. With the resulting plot, we could identify the differences between the calibrated and uncalibrated models. To compare differences in sub-basins before and after calibration, we included Kendall's tau-b correlation coefficient (τ) using the Statistical Product and Service Solutions 25 (SPSS 25) software (Arndt et al., 1999). Kendall's tau-b correlation coefficient (τ) is a statistical method used to measure the ordinal association between two measured quantities (Kendall, 1938); it ranges between -1 and 1. If $\tau > 0$, the two variables are positively correlated, and $\tau < 0$ indicates a negative correlation. The larger the absolute value of the correlation coefficient, the closer the correlation between the two variables (Bazyar et al., 2016). The strength of the correlation was considered perfect if $\tau = 1$. We defined $0.7 \leq \tau < 1$ as a strong correlation, $0.5 \leq \tau < 0.7$ as a moderate correlation, and $0.3 \leq \tau < 0.5$ as a weak correlation, following the study of Bazyar et al. (2016). Second, we visualized the changes by mapping the three CSA classes (high risk, potential risk, and low risk) to see the changes in CSA locations. As a third step, we made a comparison table to identify the similarities between the two calibrated and uncalibrated models. The comparison table is inspired by the confusion matrix (Stehman, 1997) and presents a two-by-two matrix indicating the percentages of similarities and dissimilarities between CSAs and non-CSAs before and after calibration (Table S6). If the sum of the 'both CSAs' and 'both non-CSAs' sub-basin number fell within the range of 90%–100%, we categorized the usage of the uncalibrated model to identify the CSAs as 'good', while a range from 75% to 90% was considered 'satisfactory', and <75% was 'unsatisfactory'.

3. Results

3.1. Model simulations for streamflow, sediment, and nutrient loads

To compare the calibrated and uncalibrated model results, we first calibrated the model. Table S4 shows the model's performance after calibration for both the calibration and validation periods. The R^2 and NSE of almost every variable reached a degree of at least satisfactory according to Moriasi et al. (2015), while the Pbias did not always reach this level. Since we paid more attention to the relative changes in sub-basin output before and after calibration, the whole performance of the simulation is acceptable and can be used in the study area. Statistics

regarding the model uncertainties of calibrated and uncalibrated models for streamflow, sediment, TN, and TP can be seen in Table S7. Regarding streamflow simulation uncertainty, 79%–93% of the measured data were bracketed by the 95% uncertainty band during the simulation period, and the R-factor (1.15–1.36) was within an acceptable range. For sediment, 65% of the observed data were bracketed by the 95% uncertainty bands, and the R-factors for both calibration and validation periods were less than 1. Both of the 95% observed data for TN and TP loads were bracketed by the 95% uncertainty band for the calibration period, and the R-factors were 1.36 and 1.04 for TN and TP, respectively. For the validation period of TN and TP, the P-factors were 47%–72% for TN and TP, and the R-factors were less than 1.

Fig. S2 shows monthly data for streamflow, sediment, TN, and TP for the whole study period. The observations and simulations are close and show the same dynamics. We adjusted the hydrological process and peaks by calibration, resulting in large Pbias values. For all variables, there is a clear peak around August every year. For TN, there are two peaks: one smaller peak occurs around April, and a larger peak occurs around August. In addition, Fig. S3 shows that each of the four variables had lower peaks in the dry year (2011) compared to the normal (2012) and wet year (2013).

The output of the monthly variable simulation is consistent with the rainfall pattern; the highest loads are in flood seasons (see Fig. S3). However, there are some differences, mainly in the timing of the peaks. The peak of streamflow, sediment, TN, and TP is one month later than the rainfall peak. During the flood seasons, the order of the highest monthly load simulations are: dry year < normal year < wet year. The difference between the peaks of rainfall and the four variables makes the calibration difficult. Both the observation data of the monitoring station and the model output present uncertainties, and the influence of rainfall and other input data on the simulation results should also be taken into account.

3.2. Identifying CSAs of sediment and nutrient loads on an annual scale

To determine how the contributions of sediment and nutrient loads from each sub-basin changed before and after calibration on a yearly scale, the average values from 2011 to 2013 were compared (Fig. 2). Ideally, the contributions of the sub-basins to the total loads would fit the 1:1 line. The larger the change of the sub-basins' contribution after calibration, the further the distance of points from this line. According to the position of these points on the coordinate axis, a regression equation was fitted for sediment, TN, and TP. R^2 represents the goodness of fit of the regression equation. Fig. 2a shows how the calibration process influences the contribution of the sediment load in the sub-basins. The points are positively correlated, with $R^2 = 0.78$, indicating that there is a good relationship between the sediment load contributions before and after calibration. For TN (Fig. 2b), the points also form a positive correlation but are more scattered ($R^2 = 0.48$). This indicates that, to a certain extent, the TN contribution may change based on the calibration. The total correlation of the TN contribution is close to the 1:1 line. For TP, all points are concentrated around the 1:1 line, forming a good linear relationship ($R^2 = 0.96$; Fig. 2c). In statistics, the Kendall rank correlation coefficient showed that the sub-basins' contribution for TP, TN, and sediment shows a significant correlation between calibrated and uncalibrated models ($p < 0.001$). TP and sediment are strongly correlated (TP: $\tau = 0.89$; sediment: $\tau = 0.76$), and TN is moderately correlated ($\tau = 0.61$). This shows that the calibration process has less effect on the simulated contribution of TP and sediment load than that of TN in each sub-basin.

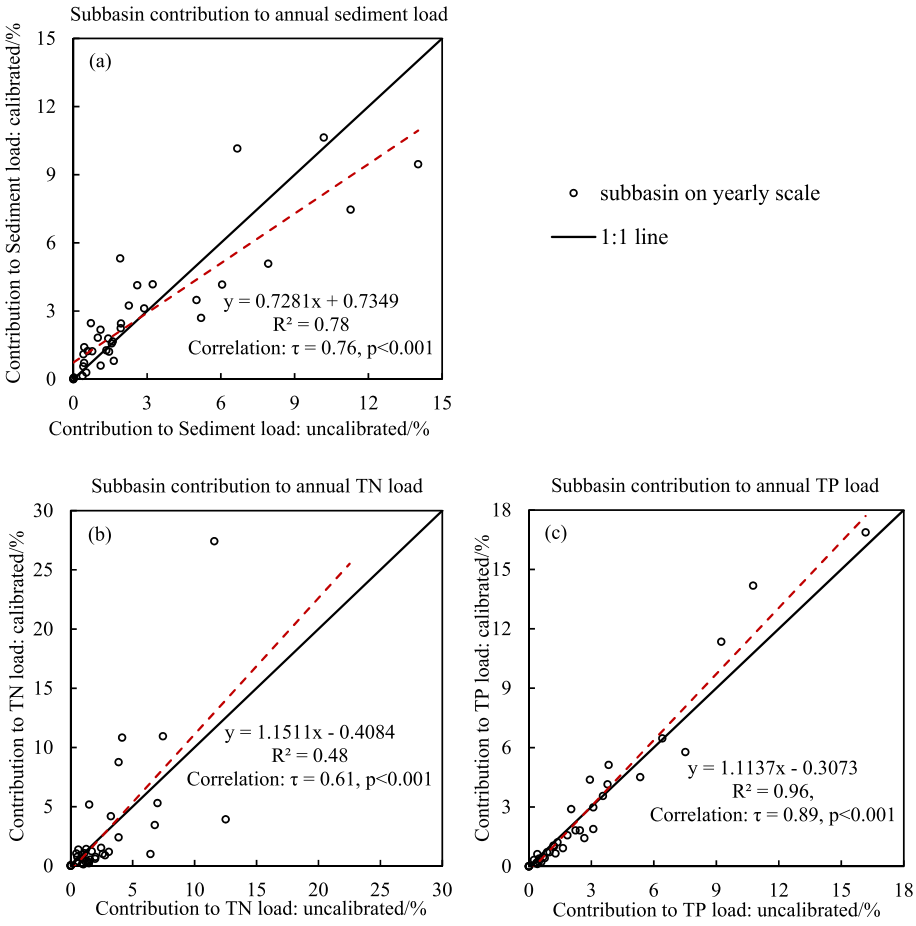

Fig. 2. Fengyu sub-basin contributions (%) to annual loads before and after calibration: (a) for sediment, (b) for TN, and (c) for TP.

Fig. 3 shows the location of CSAs in different classes. Here, we focus on the first three levels of the CSA classifications. For sediment, most CSA locations before and after calibration are similar. Sediment CSAs are mainly concentrated in the north and middle parts of the watershed. For TN, before calibration, most CSAs appeared in the north and middle parts; after calibration, the major loads of TN were concentrated in fewer sub-basins in the middle part of the watershed. All CSAs for TN after calibration overlapped with those before calibration, but compared to the uncalibrated model, half of the CSAs were not identified after calibration. The level of CSAs for TN also changed notably after calibration. Calibration changed the locations and levels of the CSAs for TP very little. We can see that the classification of TP CSAs is consistent before and after calibration. In sum, Fig. 3 shows that, on a yearly scale, the locations of CSAs for sediment and TP that appear after calibration are similar to those before calibration. For TN CSAs, the number of areas decreased considerably after calibration, but those remaining after calibration overlapped with the uncalibrated results.

The comparison matrix (Table 1) shows the similarities of sub-basin classification in CSA numbers and locations. For sediment after calibration, 19% of the sub-basins changed from CSAs to non-CSAs or vice versa, and 81% of the sub-basins did not change to be CSAs or non-CSAs. No new CSAs for TN and TP were identified after calibration; the number only decreased. Of the sub-basins for TN, 27% transformed from CSAs to non-CSAs (this equates to a 62% reduction in TN CSAs after calibration), and 10% of the sub-basins for TP transformed from CSAs into non-CSAs. In total, the unchanged sub-basins of CSAs or non-CSAs for TN and TP were 73% and 90%, respectively. The calibration process has less impact on sediment and TP CSA identification compared with TN.

Table 1
Percentage (%) difference before and after calibration in model results for nutrients (TN and TP) and sediment loads for CSAs and non-CSAs (yearly results).

After Calibration / Before Calibration	Sediment		TN		TP	
	CSAs	Non-CSAs	CSAs	Non-CSAs	CSAs	Non-CSAs
CSAs	30	5	16	27	22	10
Non-CSAs	14	51	0	57	0	68

3.3. Identifying CSAs of sediment and nutrient loads on a seasonal scale

Fig. 4 shows how the sub-basins' contributions changed before and after calibration on a seasonal scale. The three figures show the contributions of the three variables in six hydrological conditions. On the seasonal scale, the goodness of fit of the regression equation for each variable performed less well than the annual scale, as R^2 is less than the yearly scale. As Fig. 4 shows, there are seasonal differences in the contributions of the sub-basins, as most that have larger values for load contribution correspond to the flood season. However, for TN after calibration, some sub-basins in the non-flood season tend to have a higher load contribution than before calibration (see the grey, blue, and dark blue dots in Fig. 4b). The points for TN are scattered more than sediment and TP, and TP has a higher R^2 (0.86) than sediment (0.74) and TN (0.30). The correlation analysis showed that the sub-basins' contributions of sediment, TN, and TP before and after calibration were still significantly correlated at the seasonal scale. The correlation coefficients, in descending order, are TP ($\tau = 0.79$), Sediment ($\tau = 0.66$),

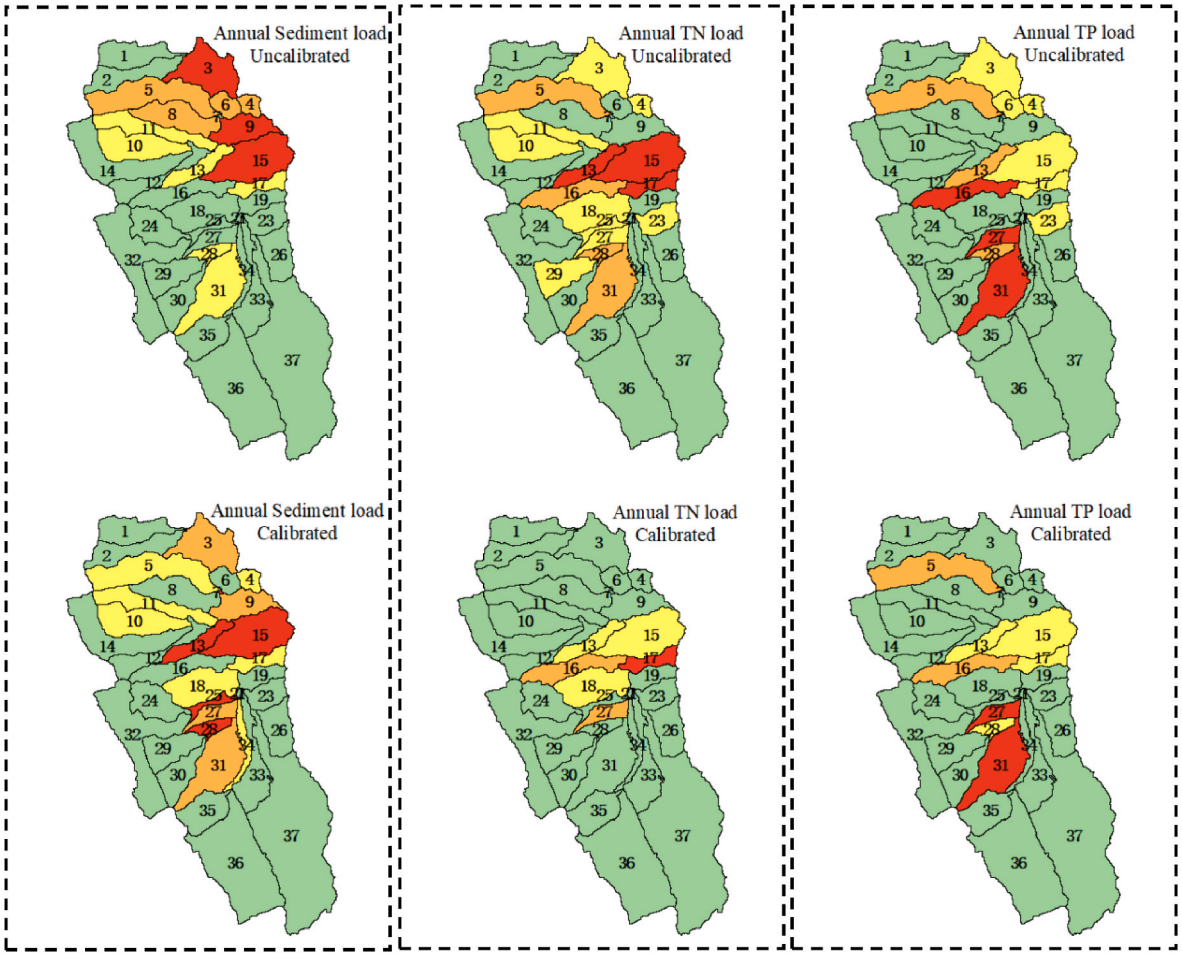

Fig. 3. Nutrient and sediment loads from Fengyu sub-basins, as calculated by the calibrated and uncalibrated models (the first-level CSAs are in red; second-level CSAs are in orange; and the potential pollution source areas are in yellow).

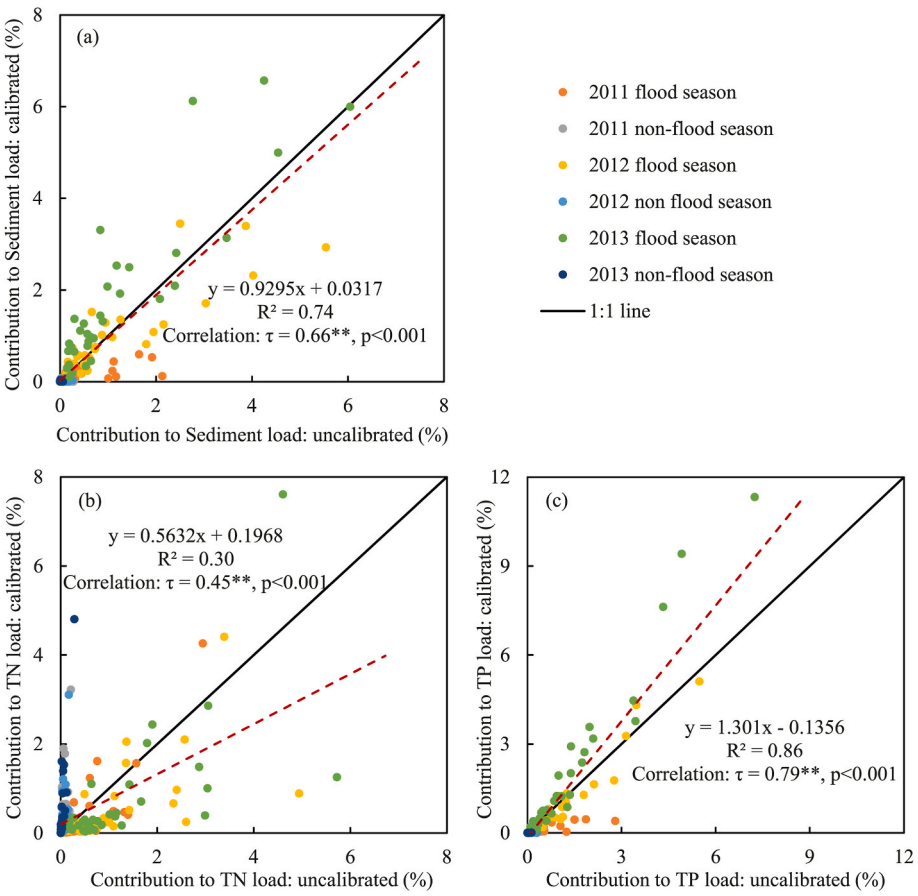

Fig. 4. Fengyu sub-basin contributions to seasonal loads before and after calibration: (a) for sediment, (b) for TN, and (c) for TP.

and TN ($\tau = 0.45$). After calibration, the contribution of TN by sub-basin in non-flood seasons shows larger values, this change scatters the points and reduces its correlation on the seasonal scale.

We marked the seasonal CSA locations of each variable on the map (Fig. 5). The results of the CSAs regarding sediment show few differences between the calibrated and uncalibrated model results. All the CSAs only appear in the flood season, and the locations are similar to the yearly scale. For TN, before calibration, all CSAs are present in flood seasons. They are mainly concentrated in the normal and wet years with the same sub-basin locations. However, after calibration, CSAs are more evenly distributed over the seasons. The CSAs for TN after calibration are distributed in the middle of the watershed and in almost the same locations in each hydrological season. For TP, all the CSAs tend to appear in the flood season; however, the number of CSAs is less than that of the uncalibrated result. When we compare the locations of the CSAs for TP, it is clear that the locations before and after calibration are similar. Furthermore, the classification of most CSA sub-basins is also consistent.

Table 2 is a comparison table on a seasonal scale. It shows that most sub-basins remained as CSAs or non-CSAs. For TP, 7% of the sub-basins became non-CSAs after calibration. The other 93% (7% for 'both CSAs' and 86% for 'both non-CSAs') of sub-basins did not change. For sediment, the CSA locations and numbers were almost the same before and after calibration (with a similarity of 90%). The table shows that 10% of the sub-basins are identified as sediment CSAs by both calibrated and uncalibrated models, and 80% were non-CSAs by both models. Additionally, 5% of sub-basins were solely identified as sediment CSAs by the uncalibrated model, and 5% of sub-basins for sediment were identified as CSAs after calibration but not before calibration. For TN, the sub-basins changed significantly between CSAs and non-CSAs (16%). This means that the CSAs for TN decreased by 56% after calibration and added about 43% new sub-basins in the non-flood season, which indicates that the uncalibrated model is less accurate in identifying CSAs for TN. There are four forms of nitrogen from three sources. To explore the reasons for the changes in CSAs after calibration in non-flood seasons, we calculated the sources of total nitrogen in non-flood seasons before and after calibration. After calibration, we found that the contribution of NO_3^- in groundwater to TN increased substantially: the contribution of groundwater flow to nitrogen changed from 2% of the total nitrogen flow in the non-flood season before calibration to 34% after calibration.

4. Discussion

This study took the Fengyu River Watershed as a case study to explore whether a model without calibration could effectively identify CSAs for sediment, TN, and TP. We discuss our results from the calibration of the SWAT model, the relative contribution of sub-basins to nutrients and sediment load, the differences in CSA locations between the calibrated and uncalibrated models, and the percentage change for CSAs and non-CSAs; we also examine possible explanations. Subsequently, considerations about whether the uncalibrated model can be used to evaluate CSAs in watershed water management are presented.

4.1. Model calibration and performance

We started our research with model calibration on the four variables (streamflow, sediment, TN, and TP). With the outcomes, we aimed to identify the overall effect of calibration visually and statistically. First, the observation and simulation values are close to each other. According to the visible match between the lines, it is clear that the dynamics and the peak timing sometimes differed but did so in an acceptable range. Second, given the good values for the R^2 and NS, the calibration results

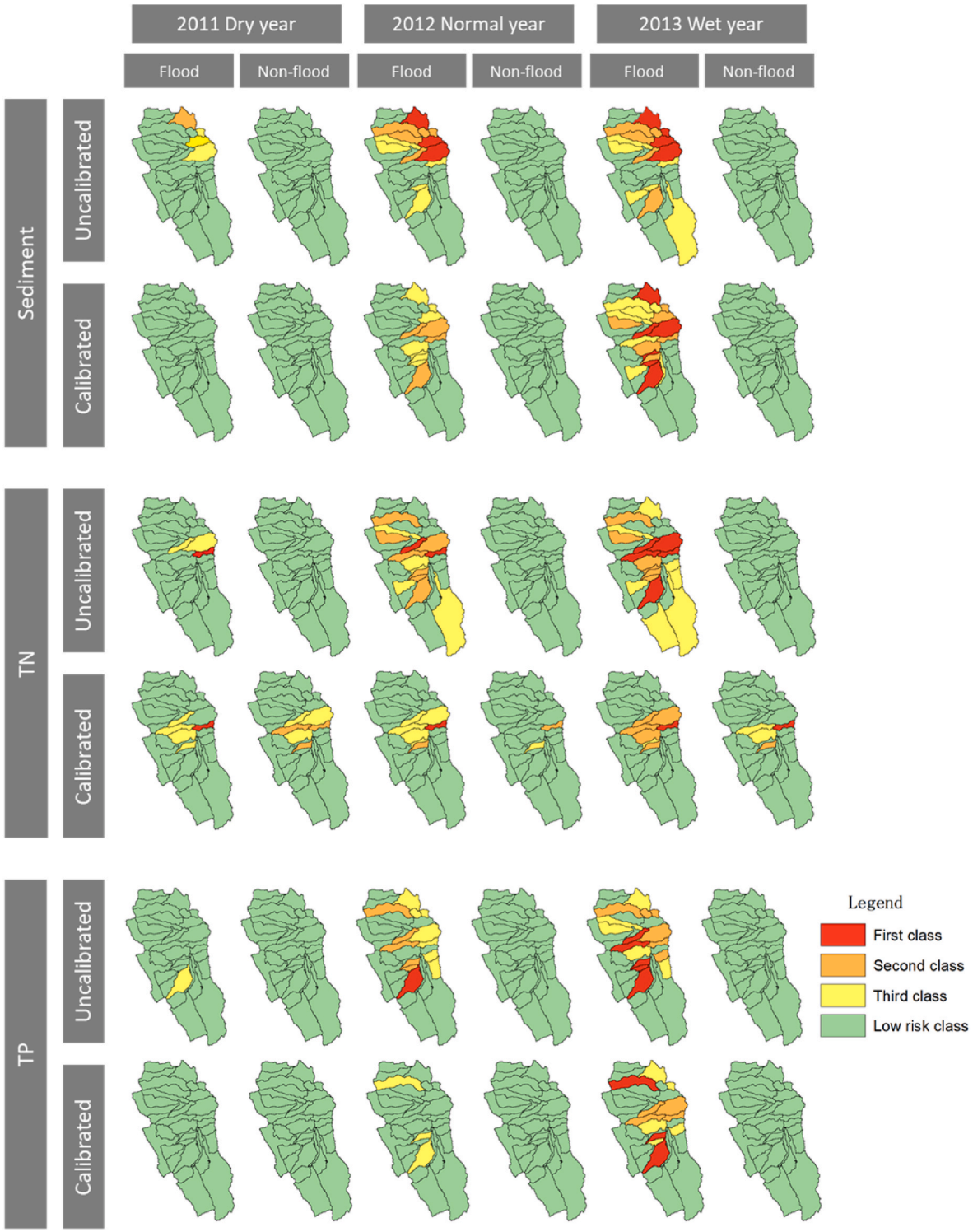

Fig. 5. Classification of sediment, TN, and TP loads from each Fengyu sub-basin based on the calibrated and uncalibrated models (the first-level CSAs appear in red; second-level CSAs are in orange; and potential pollution source areas appear in yellow). (For interpretation of the references to colour in this figure legend, the reader is referred to the Web version of this article.)

are also acceptable, especially since this study mainly focuses on relative values. However, in 2013, the rainfall peak was in July, while the four variables' peaks were all in September, which the calibrated model did not capture well. In the calibration process, we adjusted the runoff parameters to reduce the contribution of surface runoff and increase the contribution of groundwater compared to the uncalibrated model, thereby reducing the contribution of rainfall to runoff. It is also important to note that our study only concerns a period of three years. According to probability theory, a smaller sample may lead to more errors (Kraaikamp and Meester, 2005; Yao and Gao, 2015, Shang et al., 2012, Yuan et al., 2019). Other studies based on SWAT in the Erhai Basin have also shown that a limiting the number of years included in the calibration (e.g., Shang et al., [2012]Shang et al., [2012]) results in a lower agreement between observation and simulation than when more

Table 2
Percentage (%) difference before and after calibration in model results for nutrients (TN and TP) and sediment loads for CSAs and non-CSAs (seasonal results).

After Calibration Before Calibration	Sediment		TN		TP	
	CSAs	Non-CSAs	CSAs	Non-CSAs	CSAs	Non-CSAs
CSAs	10	5	7	9	7	7
Non-CSAs	5	80	7	77	0	86

years are used (e.g., Yuan et al., [2019]Yuan et al., [2019]).

4.2. Contribution of each subbasin

To investigate the effect of calibration on sub-basins' contribution changes, we compared the sub-basins' relative contribution to the loads before and after calibration (Figs. 2 and 4). Both figures show that the TN contribution changed significantly. In the SWAT model, the load of TN is calculated as the sum of organic nitrogen and inorganic nitrogen (including nitrate in the surface runoff, nitrate in the lateral flow, and nitrate in groundwater). In the calibration process, we adjusted the proportion of each source in the streamflow. With this approach, the contribution of groundwater exceeded the surface runoff and lateral flow; this is why the CSAs changed more after calibration. However, sub-basins with a higher TN contribution before calibration, may maintain high contributions after calibration. For sediment, the sub-basins' contribution points before and after calibration are close to the 1:1 line, forming a better linear relationship. However, sediment is greatly affected by surface runoff and is less related to groundwater. This may explain why calibration changes some locations for sediment to a certain extent. For TP, the model predicted similar sub-basins contributions independent of whether it was calibrated. This could be explained by the higher importance of the surface water flow of TP compared to the importance of groundwater for TN. The sources of TP are mainly carried by surface runoff and the channel itself. Thus, TP output also showed limited changes at the yearly and seasonal scales due to calibration.

4.3. The use of uncalibrated models to identify CSA locations

In our study, CSAs changed spatial-temporally, which is consistent with the results of other studies (Guo et al., 2020; Shrestha et al., 2021; Uribe et al., 2020; Wei et al., 2016). Here, we explored whether SWAT without calibration can be used to identify CSAs. Our results indicate that using an uncalibrated model to identify CSAs for TP is reliable, and for sediment, it is sufficient. Using uncalibrated models for TN seems inadvisable in our case. Niraula et al. (2012) have concluded that an uncalibrated model can be used for TN, as well. This conclusion may result from the fact that their study area is less affected by groundwater, leading to more homogeneous conditions. Moreover, we differentiate among seasons, while Niraula et al. (2012) identified CSAs over the course of the year, which also led to less variation. There are other differences between our study and that of Niraula et al. (2012), as well. First, the spatial scale of Niraula et al. (2012) is based on the HRU scale. For water management, our approach using the sub-basin scale is convenient for implementing management practices to control water quality. Second, the CSA classification is different. Niraula et al. (2012) defined the top 20 HRUs as CSAs, but our study uses different levels of CSAs, classifying sub-basins as contributing to the top 20%, 40%, and 60%. We argue that the choice of CSAs is arbitrary and depends on the level of detail required.

With respect to the number of sub-basins that are CSAs before and after calibration, we found that, at the yearly scale, the number of CSAs for TN and TP decreased by 27% and 10%, respectively (Table 1), after calibration. For sediment, TN, and TP, the seasonal scale showed that 90%, 84%, and 93%, respectively of sub-basins did not change their status for CSAs and non-CSAs combined. Although this result seems satisfactory, we note that the majority of the basins belongs to the non-CSAs. Therefore, changes in CSAs may not be fully reflected in the combined percentage of unchanged values because they are biased towards the non-CSAs. When focusing purely on total changed CSAs, sediment and TP performed well.

4.4. Potential factors that could affect differences between model predictions

Here, we used a single model with the same input but changed parameters by calibration. Accordingly, we saw a change in CSA locations. CSAs can change for other reasons, too, though. For example, changes in model input or model structure may also result in different CSAs. For example, Evenson et al. (2021) used four versions of SWAT and one version of SPARROW and showed different CSAs.

The initial thresholds of all parameters and the optimal parameters after calibration are shown in Table S3. Streamflow is mainly derived from surface runoff, lateral flow, and return flow. Before calibration, the default model indicates that the groundwater flow may be low. Therefore, parameters related to the production of flow were manually adjusted based on automatic calibration. Calibration mainly reduces surface runoff, increases soil infiltration capacity and vegetation transpiration, and increases the proportion of groundwater flow.

The river channel and groundwater flow are the sources of sediment load, but they do not contribute much to total sediment production. Sediment mainly comes from soil loss caused by surface runoff. Surface runoff mainly occurs in the flood season when rainfall is concentrated, so the calibrated sediment yield is also concentrated then. The SWAT model calculates soil loss using the universal soil loss equation (USLE). The two parameters, USLE_C and USLE_P, in the USLE equation are relatively sensitive (ranked 4 and 2 of the 42 parameters), which reduced the overall sediment yield of the calibrated sub-basin. The SWAT model calibrates by adjusting each HRU's sediment yield. The number and types of HRUs in each sub-basin are different. Therefore, the contribution of sub-basins' sediment yield partly differs after calibration; even the overall sediment yield of all sub-basins decreases.

The parameters related to nitrogen and phosphorus are mainly related to the transport and transformation process of different forms of nitrogen and phosphorus and the ratio of adsorption to sediment. Therefore, beyond the overall reduction after calibration, there are also differences between sub-basins. In addition to surface runoff, the main source of total nitrogen is groundwater flow. Model calibration can increase the proportion of groundwater flow, and changes in the contributions of surface runoff and groundwater flow to streamflow on an annual scale have limited effects on sediment and nutrient output. However, when we divided the data into the flood season and the non-flood season, the difference became apparent. This is because the main contribution to streamflow in the flood season is surface runoff, and the main contribution to streamflow in the non-flood season is from groundwater flow. Therefore, after calibration, sediment and TP have almost no CSAs in non-flood seasons, while TN has CSAs in non-flood seasons because groundwater flow provides a pathway for TN then.

4.5. Implications for management

Our results can provide a different view of watershed management on both the yearly and seasonal scales. On the yearly scale, the majority did not change in terms of CSA identification before and after calibration. Managing the water quality in the watershed can rely on these unchanged sub-basins because the focus and investments concern those regions that pollute the most while omitting non-CSAs. Moreover, none of the non-CSAs for TN became CSAs after calibration, which is also beneficial for management, as this procedure will not omit CSAs that the uncalibrated model indicates are non-CSAs. Following similar reasoning, the uncalibrated model can identify most CSAs for sediment.

However, using an uncalibrated model to identify sediment CSAs runs a risk of managing the wrong regions. For TP, management could rely more on the uncalibrated model then for sediment.

For the seasonal scale, sediment load in the sub-basins in the non-flood seasons is very low, and higher values only appear in the flood seasons. Since the Fengyu River Watershed should reduce the sediment load, sediment management should focus on flood seasons and wet years in which rainfall events and stormflow occur. For TN, seasonal rainfall determines the number and level of the CSAs in the uncalibrated model. Therefore, CSAs are only present in flood seasons and are lacking in non-flood seasons in the uncalibrated model. However, the calibrated model shows CSAs in both flood and non-flood seasons, with a similar pattern between the two. Therefore, there is no need to calculate CSAs on the seasonal scale for TN. If CSAs are calculated with the uncalibrated model, the results seem useful for management for the flood season only For sediment and TP, the situation is different. In both the uncalibrated and calibrated models, the load is high in rainy seasons. Therefore, all the CSAs were identified independently by the calibrated and uncalibrated models, and management can thus rely on uncalibrated results on the seasonal scale for sediment and TP. To improve the management value of CSAs identified by uncalibrated models, future studies should include high-resolution databases, long time series with observed data, and rainfall and streamflow with a similar trend. Moreover, by providing more case studies, we can improve our knowledge of uncalibrated model results to identify CSAs in management.

5. Conclusions

Our study used the SWAT model to verify the feasibility of using the uncalibrated model to identify CSAs. We considered six different hydrological conditions that reflected the inter-annual and seasonal variations to investigate the differences between CSAs identified with the calibrated and uncalibrated models. Overall, our results showed that the modelled nutrient loads can substantially change after model calibration. The locations of CSAs for sediment, phosphorus, and nitrogen under different hydrological conditions and the changes of CSAs before and after calibration successfully captured the yearly and seasonal differences. For sediment and TP CSAs, more than 90% of the sub-basins remain CSAs or non-CSAs before and after calibration achieved 'good' similarity results. TN had a lower similarity than TP and sediments, and TN CSAs showed acceptable results on both yearly and seasonal scales. The model results suggest that water yield composition is changed by calibration with an increase in the surface runoff and a decrease in the groundwater flow. The groundwater flow's contribution to nitrogen increased substantially in the non-flood season after calibration, leading to TN CSAs appearing in the non-flood season. Our calibrations resulted in large adjustments to the water balance. In situations when the water yield composition changes are limited, the performance of TN could improve. For sediment and TP, their loads are mainly related to surface runoff. The water yield adjustments did not influence the TP and sediment load. Our results suggest there is a relative agreement between the two calibrated and uncalibrated models in identifying CSAs. For further research, we recommend focusing more on multiple sources when using an uncalibrated model to identify nutrient CSAs, as nutrients such as TN from different sources would contribute differently after calibration. Moreover, the effect of groundwater flows in the identification of CSAs should be considered when using uncalibrated models.

Credit author statement

Meijun Chen: Conceptualization, Formal analysis, Writing – original draft, Revising. Annette B. G. Janssen: Supervision, Formal analysis, Writing – review & editing. Jeroen J. M. de Klein: Supervision, Formal analysis, Writing – review & editing. Xinzhong Du: Supervision, Formal analysis, Writing – review & editing. Qiuliang Lei: Supervision, Formal analysis, Writing – review & editing. Ying Li: Data collection, Writing – review & editing. Tianpeng Zhang: Data collection, Writing – review & editing. Wei Pei: Data collection, Writing – review & editing. Carolien Kroeze: Supervision, Formal analysis, Writing – review & editing. Hongbin Liu: Supervision, Formal analysis, Writing – review & editing.

Declaration of competing interest

The authors declare that they have no known competing financial interests or personal relationships that could have appeared to influence the work reported in this paper.

Data availability

Data will be made available on request.

Acknowledgements

The work of MC is supported by the National Natural Science Foundation of China (Grant No#42107076; Grant No#U20A20114), ABGJ is supported by the NWO talent grant Veni (project number VI. Veni.194.002) and the KNAW project SURE+ (PSA-SA-E-01). This study is also supported by China Scholarship Council (CSC) and the Joint PhD Program in Agriculture and Life Science between the Graduate School of Chinese Academy of Agricultural Sciences (GSCAAS) and the University of Wageningen.

Appendix A. Supplementary data

Supplementary data to this article can be found online at https://doi.org/10.1016/j.jenvman.2022.116712.

References

Abbaspour, Karim.C., 2013. SWAT-CUP 2012: SWAT calibration and uncertainty programs–a user manual. Eawag, Dübendorf, Switzerland.
Andersen, H.E., Kronvang, B., 2006. Modifying and evaluating a P index for Denmark. Water Air Soil Pollut. 174, 341–353. https://doi.org/10.1007/s11270-006-9123-0.
Arndt, S., Turvey, C., Andreasen, N.C., 1999. Correlating and predicting psychiatric symptom ratings: spearmans r versus Kendalls tau correlation[J]. J. Psychiatr. Res. 33 (2), 97–104. https://doi.org/10.1016/S0022-3956(98)90046-2.
Arnold, J.G., Kiniry, J.R., Srinivasan, R., Williams, J.R., Haney, E.B., Neitsch, S.L., 2013. SWAT 2012 Input/Output Documentation. Texas Water Resources Institute. Available electronically from. https://hdl.handle.net/1969.1/149194.
Bazyar, S., Ramalho, J., Eldeniz, C., et al., 2016. Comparison of cerebral blood volume and plasma volume in untreated intracranial tumors[J]. PLoS One 11 (9), e0161807. https://doi.org/10.1371/journal.pone.0161807.
Bouraoui, F., Dillaha, T.A., 1996. ANSWERS-2000: runoff and sediment transport model. J. Environ. Eng. 122, 493–502. https://www.oieau.org/eaudoc/system/files/documents/9/46887/46887_doc.pdf.
Chen, H., Luo, Y., Potter, C., et al., 2017. Modeling pesticide diuron loading from the san joaquin watershed into the sacramento-san joaquin delta using SWAT[J]. Water Res. 121, 374–385. https://doi.org/10.1016/j.watres.2017.05.032.
Chen, X., Strokal, M., Van Vliet, M.T.H., Stuiver, J., Wang, M., Bai, Z., Ma, L., Kroeze, C., 2019. Multi-scale modeling of nutrient pollution in the rivers of China. Environ. Sci. Technol. 53, 9614–9625. https://doi.org/10.1021/acs.est.8b07352.
Davies, G., 2019. Tsunami variability from uncalibrated stochastic earthquake models: tests against deep ocean observations 2006–2016. Geophys. J. Int. 218, 1939–1960. https://doi.org/10.1093/gji/ggz260.
Drewry, J.J., Newham, L.T., Croke, B.F., 2009. Suspended sediment, nitrogen and phosphorus concentrations and exports during storm-events to the Tuross estuary, Australia. J. Environ. Manag. 90, 879–887. https://doi.org/10.1016/j.jenvman.2008.02.004.
Du, X., Shrestha, N.K., Wang, J., 2019. Integrating organic chemical simulation module into SWAT model with application for PAHs simulation in Athabasca oil sands region, Western Canada[J]. Environ. Model. Software 111, 432–443. https://doi.org/10.1016/j.envsoft.2018.10.011.
Evenson, G.R., Kalcic, M., Wang, Y.C., et al., 2021. Uncertainty in critical source area predictions from watershed-scale hydrologic models[J]. J. Environ. Manag. 279, 111506 https://doi.org/10.1016/j.jenvman.2020.111506.
GB3838-2002, 2002. Chinese National Environmental Quality Standards for Surface Water. Ministry of Environmental Protection. https://www.mee.gov.cn/ywgz/fgbz/bz/bzwb/shjbh/shjzlbz/200206/t20020601_66497.htm.
Ghebremichael, L.T., Veith, T.L., Watzin, M.C., 2010. Determination of critical source areas for phosphorus loss: lake champlain basin, Vermont. T Asabe 53, 1595–1604. https://doi.org/10.13031/2013.34898.

Guo, Y., Wang, X., Zhou, L., Melching, C., Li, Z., 2020. Identification of critical source areas of nitrogen load in the miyun reservoir watershed under different hydrological conditions. Sustainability-Basel 12. https://doi.org/10.3390/su12030964.

Han, C., Xu, S., Liu, J., Lian, J., 2010. Nonpoint-source nitrogen and phosphorus behavior and modeling in cold climate: a review. Water Sci. Technol. 62, 2277–2285. https://doi.org/10.2166/wst.2010.464.

Hanjra, M.A., Qureshi, M.E., 2010. Global water crisis and future food security in an era of climate change. Food Pol. 35, 365–377. https://doi.org/10.1016/j.foodpol.2010.05.006.

Janssen, A.B.G., Janse, J.H., Beusen, A.H.W., Chang, M., Harrison, J.A., Huttunen, I., Kong, X., Rost, J., Teurlincx, S., Troost, T.A., 2019. How to model algal blooms in any lake on earth. Curr. Opin. Environ. Sustain. 36, 1–10. https://doi.org/10.1016/j.cosust.2018.09.001.

Janssen, A.B.G., de Jager, V.C.L., Janse, J.H., Kong, X., Liu, S., Ye, Q., Mooij, W.M., 2017. Spatial identification of critical nutrient loads of large shallow lakes: implications for Lake Taihu (China). Water Res. 119, 276–287. https://doi.org/10.1016/j.watres.2017.04.045.

Ji, N., Wang, S., Zhang, L., 2017. Characteristics of dissolved organic phosphorus inputs to freshwater lakes: a case study of Lake Erhai, southwest China. Sci. Total Environ. 601, 1544–1555. https://doi.org/10.1016/j.scitotenv.2017.05.265.

Kendall, M.G., 1938. A new measure of rank correlation[J]. Biometrika 30 (1/2), 81–93. https://doi.org/10.2307/2332226.

Kraaikamp, F.D.C., Meester, H.L.L., 2005. A Modern Introduction to Probability and Statistics. Springer, Berlin/Heidelberg, Germany. http://www.jjernigan.com/152/probability_text.pdf.

Li, J., Bai, Y., Alatalo, J.M., 2020. Impacts of rural tourism-driven land use change on ecosystems services provision in Erhai Lake Basin, China. Ecosyst. Serv. 42, 101081 https://doi.org/10.1016/j.ecoser.2020.101081.

Li, X., Janssen, A.B.G., de Klein, J.J.M., Kroeze, C., Strokal, M., Ma, L., Zheng, Y., 2019a. Modeling nutrients in lake dianchi (China) and its watershed. Agric. Water Manag. 212, 48–59. https://doi.org/10.1016/j.agwat.2018.08.023.

Li, Y., Yen, H., Harmel, R.D., Lei, Q., Zhou, J., Hu, W., Li, W., Lian, H., Zhu, A.-X., Zhai, L., 2019b. Effects of sampling strategies and estimation algorithms on total nitrogen load determination in a small agricultural headwater watershed. J. Hydrol. (Amst.) 579, 124114. https://doi.org/10.1016/j.jhydrol.2019.124114.

Lin, S., Shen, S., Zhou, A., Lyu, H., 2020. Sustainable development and environmental restoration in Lake Erhai, China. J. Clean. Prod. 258, 120758 https://doi.org/10.1016/j.jclepro.2020.120758.

Liu, H., Li, S., Qin, P., 2020. Study on the method of solving the P-III curve fitted by precipitation frequency based on excel[C]//IOP conference series: earth and environmental science. IOP Publishing 525 (1), 012129. http://doi:10.1088/1755-1315/525/1/012129.

McLaughlin, K.R., 1997. Hydrologic Condition Analysis[C]. Georgia Institute of Technology. http://hdl.handle.net/1853/45116.

McMahon, T.A., Srikanthan, R., 1981. Log Pearson III distribution - is it applicable to flood frequency analysis of Australian streams?[J]. J. Hydrol. 52 (1–2), 139–147. https://doi.org/10.1016/0022-1694(81)90100-1.

Moriasi, D.N., Gitau, M.W., Pai, N., Daggupati, P., 2015. Hydrologic and water quality models: performance measures and evaluation criteria. T Asabe 58, 1763–1785. https://doi.org/10.13031/trans.58.10715.

Neitsch, S.L., Arnold, J.G., Kiniry, J.R., Williams, J.R., 2011. Soil and Water Assessment Tool Theoretical Documentation Version 2009. Texas Water Resources Institute. http://twri.tamu.edu/reports/2011/tr406.pdf.

Niraula, R., Kalin, L., Srivastava, P., Anderson, C.J., 2013. Identifying critical source areas of nonpoint source pollution with SWAT and GWLF. Ecol. Model. 268, 123–133. https://doi.org/10.1016/j.ecolmodel.2013.08.007.

Niraula, R., Kalin, L., Wang, R., Srivastava, P., 2012. Determining nutrient and sediment critical source areas with swat: effect of lumped calibration. T Asabe 55, 137–147. https://doi.org/10.13031/2013.41262.

Ou, Y., Wang, X., 2008. Identification of critical source areas for non-point source pollution in Miyun reservoir watershed near Beijing, China. Water Sci. Technol. 58, 2235–2241. https://doi.org/10.2166/wst.2008.831.

Ouyang, W., Hao, F., Wang, X., 2008. Regional non point source organic pollution modeling and critical area identification for watershed best environmental management. Water, Air, Soil Pollut. 187, 251–261. https://doi.org/10.1007/s11270-007-9513-y.

Peng, J., Liu, Y., Tian, L., 2018. Integrating ecosystem services trade-offs with paddy land-to-dry land decisions: a scenario approach in Erhai Lake Basin, southwest China. Sci. Total Environ. 625, 849–860. https://doi.org/10.1016/j.scitotenv.2017.12.340.

Peters, N.E., Meybeck, M., 2000. Water quality degradation effects on freshwater availability: impacts of human activities. Water Int. 25, 185–193. https://doi.org/10.1080/02508060008686817.

Pionke, H.B., Gburek, W.J., Sharpley, A.N., 2000. Critical source area controls on water quality in an agricultural watershed located in the Chesapeake Basin. Ecol. Eng. 14, 325–335. https://doi.org/10.1016/S0925-8574(99)00059-2.

Ros, M.B.H., Ketterings, Q.M., Cela, S., Czymmek, K.J., 2019. Evaluating management implications of the New York phosphorus index with farm field information. J. Environ. Qual. 48, 1082–1090. https://doi.org/10.2134/jeq2019.01.0010.

Rozalis, S., Morin, E., Yair, Y., Price, C., 2010. Flash flood prediction using an uncalibrated hydrological model and radar rainfall data in a Mediterranean watershed under changing hydrological conditions. J. Hydrol. (Amst.) 394, 245–255. https://doi.org/10.1016/j.jhydrol.2010.03.021.

Rudra, R.P., Mekonnen, B.A., Shukla, R., Shrestha, N.K., Goel, P.K., Daggupati, P., Biswas, A., 2020. Currents status, challenges, and future directions in identifying critical source areas for non-point source pollution in Canadian conditions. Agriculture-Basel 10 (10), 468. https://doi.org/10.3390/agriculture10100468.

Shang, X., Wang, X., Zhang, D., Chen, W., Chen, X., Kong, H., 2012. An improved SWAT-based computational framework for identifying critical source areas for agricultural pollution at the lake basin scale. Ecol. Model. 226, 1–10. https://doi.org/10.1016/j.ecolmodel.2011.11.030.

Sharpley, A., Beegle, D., Bolster, C., Good, L., Joern, B., Ketterings, Q., Lory, J., Mikkelsen, R., Osmond, D., Vadas, P., 2012. Phosphorus indices: why we need to take stock of how we are doing. J. Environ. Qual. 41, 1711–1719. https://doi.org/10.2134/jeq2012.0040.

Sharpley, A.N., Kleinman, P.J.A., Flaten, D.N., Buda, A.R., 2011. Critical source area management of agricultural phosphorus: experiences, challenges and opportunities. Water Sci. Technol. 64, 945–952. https://doi.org/10.2166/wst.2011.712.

Shrestha, N.K., Rudra, R.P., Daggupati, P., Goel, P.K., Shukla, R., 2021. A comparative evaluation of the continuous and event-based modelling approaches for identifying critical source areas for sediment and phosphorus losses. J. Environ. Manag. 277, 111427 https://doi.org/10.1016/j.jenvman.2020.111427.

Stehman, S.V., 1997. Selecting and interpreting measures of thematic classification accuracy. Rem. Sens. Environ. 62, 77–89. https://doi.org/10.1016/S0034-4257(97)00083-7.

Strauss, P., Leone, A., Ripa, M.N., Turpin, N., Lescot, J.M., Laplana, R., 2007. Using critical source areas for targeting cost-effective best management practices to mitigate phosphorus and sediment transfer at the watershed scale. Soil Use Manag. 23, 144–153. https://doi.org/10.1111/j.1475-2743.2007.00118.x.

Strokal, M., Kroeze, C., Wang, M., Ma, L., 2017. Reducing future river export of nutrients to coastal waters of China in optimistic scenarios. Sci. Total Environ. 579, 517–528. https://doi.org/10.1016/j.scitotenv.2016.11.065.

Tong, X., Zhou, Y., Liu, J., Qiu, P., Shao, Y., 2021. Non-point source pollution loads estimation in Three Gorges Reservoir Area based on improved observation experiment and export coefficient model. Water Sci. Technol. 85 (1), 27–38. https://doi.org/10.2166/wst.2021.508.

Tong, Y., Bu, X., Chen, J., Zhou, F., Chen, L., Liu, M., Tan, X., Yu, T., Zhang, W., Mi, Z., Ma, L., Wang, X., Ni, J., 2017a. Estimation of nutrient discharge from the Yangtze River to the East China Sea and the identification of nutrient sources. J. Hazard Mater. 321, 728–736. https://doi.org/10.1016/j.jhazmat.2016.09.011.

Tong, Y., Zhang, W., Wang, X., Couture, R.M., Larssen, T., Zhao, Y., Li, J., Liang, H., Liu, X., Bu, X., He, W., Zhang, Q., Lin, Y., 2017b. Decline in Chinese lake phosphorus concentration accompanied by shift in sources since 2006. Nat. Geosci. 10, 507–511. https://doi.org/10.1038/ngeo2967.

Uribe, N., Srinivasan, R., Corzo, G., Arango, D., Solomatine, D., 2020. Spatio-temporal critical source area patterns of runoff pollution from agricultural practices in the Colombian Andes. Ecol. Eng. 149, 105810 https://doi.org/10.1016/j.ecoleng.2020.105810.

Wang, M., Kroeze, C., Strokal, M., van Vliet, M.T.H., Ma, L., 2020. Global change can make coastal eutrophication control in China more difficult. Earth's Future 8 (4), e2019EF001280. https://doi.org/10.1029/2019EF001280.

Wang, M., Strokal, M., Burek, P., Kroeze, C., Ma, L., Janssen, A.B.G., 2019. Excess nutrient loads to Lake Taihu: opportunities for nutrient reduction. Sci. Total Environ. 664, 865–873. https://doi.org/10.1016/j.scitotenv.2019.02.051.

Wei, P., Ouyang, W., Hao, F., Gao, X., Yu, Y., 2016. Combined impacts of precipitation and temperature on diffuse phosphorus pollution loading and critical source area identification in a freeze-thaw area. Sci. Total Environ. 553, 607–616. https://doi.org/10.1016/j.scitotenv.2016.02.138.

White, M.J., Storm, D.E., Busteed, P.R., Stoodley, S.H., Phillips, S.J., 2009. Evaluating nonpoint source critical source area contributions at the watershed scale. J. Environ. Qual. 38, 1654–1663. https://doi.org/10.2134/jeq2008.0375.

Wu, L., Gao, J., Ma, X., Li, D., 2015. Application of modified export coefficient method on the load estimation of non-point source nitrogen and phosphorus pollution of soil and water loss in semiarid regions. Environ. Sci. Pollut. Res. 22, 10647–10660. https://doi.org/10.1007/s11356-015-4242-z.

Yang, J., Strokal, M., Kroeze, C., Wang, M., Wang, J., Wu, Y., Bai, Z., Ma, L., 2019. Nutrient losses to surface waters in Hai He basin: a case study of Guanting reservoir and Baiyangdian lake. Agric. Water Manag. 213, 62–75. https://doi.org/10.1016/j.agwat.2018.09.022.

Yao, K., Gao, J., 2015. Law of large numbers for uncertain random variables. IEEE Trans. Fuzzy Syst. 24, 615–621. https://doi.org/10.1109/TFUZZ.2015.2466080.

Yuan, Z., Xu, J., Meng, X., Wang, Y., Yan, B., Hong, X., 2019. Impact of climate variability on blue and green water flows in the Erhai Lake Basin of Southwest China. Water 11 (3), 424. https://doi.org/10.3390/w11030424.